Long-Life Electrons in Metal-Doped Alkali-Metal Tantalate Photocatalysts Excited under Water

Fu, Zhebin
Hirai, Takuya
Onishi, Hiroshi

(Citation)
Journal of Physical Chemistry C,125(48):26398-26405

(Issue Date)
2021-11-22

(Resource Type)
journal article

(Version)
Version of Record

(URL)
https://hdl.handle.net/20.500.14094/90008901

THE JOURNAL OF PHYSICAL CHEMISTRY C
A JOURNAL OF THE AMERICAN CHEMICAL SOCIETY

pubs.acs.org/JPCC

Article

Long-Life Electrons in Metal-Doped Alkali-Metal Tantalate Photocatalysts Excited under Water

Zhebin Fu,* Takuya Hirai, and Hiroshi Onishi*

Cite This: *J. Phys. Chem. C* 2021, 125, 26398–26405

Read Online

ACCESS | Metrics & More | Article Recommendations | Supporting Information

ABSTRACT: Conversion of materials for artificial photosynthesis is completed in milliseconds or seconds by assembling atoms over semiconductor photocatalysts. Band-gap-excited electrons and holes reactive on this time scale are key for efficient atom assembly to yield the desired products. In this study, attenuated total reflection of infrared (IR) light was applied to characterize the electronic absorption of long-life charge carriers excited under water. Under excitation, $NaTaO_3$ and $KTaO_3$ photocatalyst particles doped with Sr or La cations absorbed IR light. A broad absorption band appeared with a maximum at 1400 cm^{-1}, which was enhanced by the addition of hole scavengers (e.g., methanol and Na_2SO_3) and disappeared in the presence of electron scavengers (e.g., $FeCl_3$, $NaIO_3$, and H_2O_2). This absorption corresponded to the electronic transition of band-gap-excited electrons accommodated in mid-gap states. In anaerobic *n*-decane, the electron absorption was enhanced by the excitation light power, *P*, with absorbance being proportional to $P^{1/2}$. The observed 1/2-order power law suggested deexcitation via recombination of electrons and holes. When the excitation light was stopped, the absorbance decreased as a function of time with a second-order rate law, as expected in the case of recombinative deexcitation. In addition, the 1/2-order power law and second-order decay rate law were observed in anaerobic water, with an accelerated decay rate, which was possibly due to a water-related electron-consuming reaction. This study demonstrated that long-life electrons contribute to surface redox reactions over semiconductor photocatalysts for artificial photosynthesis.

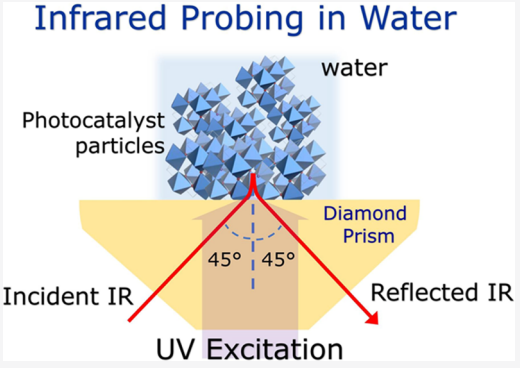

1. INTRODUCTION

Artificial photosynthesis over semiconductor photocatalysts has been extensively investigated.[1] However, light-energized material conversion has not been understood completely. Pulsed light sources and optical probing methods developed in the recent decades have helped us to determine the initial fate of the electrons and holes excited in semiconductors. Photon absorption and electronic excitation are followed by exciton formation or separation; subsequently, charge-carrier transport occurs from the bulk to the surface.[2] These electron-based steps are initiated in femtoseconds and completed in microseconds. On the other hand, reaction products are formed in milliseconds or even seconds via the assembly of atoms on the surface.[3] Hence, excited electrons and holes still reactive on that time scale are crucial to efficient atom assembly for yielding the desired products. In this study, $NaTaO_3$ and $KTaO_3$ doped with Sr or La cations were band-gap-excited to demonstrate that excited electrons are resident for 200 s under water and are reactive in redox reactions.

Excited electrons and holes absorb IR or visible light according to the host semiconductors in which they are created. As electron-induced IR absorption has been reported for $NaTaO_3$[4,5] and $KTaO_3$[6] photocatalysts excited in vacuum, electrons excited under water are to be probed by IR absorption. This was a difficult task since water absorbs IR light for probing, while excitation light is absorbed by photocatalyst particles. An attenuated total reflection (ATR) assembly with a diamond prism is key for guiding the excitation light to the volume probed by IR light. Optical absorption of TiO_2,[7,8] Fe_2O_3,[9] and $BiVO_4$[10] photoexcited in water has been characterized using a transmitted probe light, for which the materials of interest should be prepared as films exhibiting good optical transmission. Earlier studies[11−16] have conducted ATR-IR spectroscopy to detect the vibrational absorption of intermediate chemical species for photocatalytic water splitting. In this study, attention is focused on electronically excited states in photocatalyst particles that can be used for overall water splitting.[17]

2. METHODS AND MATERIALS

An isosceles-trapezoidal diamond prism with a circular reflection plane 1.8 mm in diameter was assembled by Jasco

Received: July 26, 2021
Revised: November 8, 2021
Published: November 22, 2021

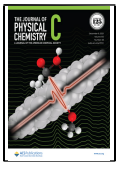

https://doi.org/10.1021/acs.jpcc.1c06618
J. Phys. Chem. C 2021, 125, 26398−26405

with an light-emitting diode (LED) (M285L5, Thorlabs). Ultraviolet (UV) light (center wavelength: 285 nm) was guided through the prism and focused on the reflection plane with a quartz lens, as illustrated in the TOC graphic. The angle of IR-light incidence θ was fixed at 45° from the normal of the reflection plane. The UV-light power on the plane was calibrated to 0.8−19 W m^{-2} using a photodiode sensor (PD-300, Ophir).

Photocatalyst particles were placed on the reflection plane and covered with a liquid droplet (typical volume: 0.25 mL). The prism assembly was set in an Fourier-transform infrared spectroscopy (FTIR) spectrometer (FT/IR-6600, Jasco) capable of rapid interferometer scans (acquisition time: 50 ms per spectrum). The reflection plane was irradiated with He−Ne laser light (wavelength: 633 nm) for interferometer calibration, which was unable to excite the photocatalysts. The prism assembly inside the spectrometer was exposed to air or N_2 gas to make the droplet anaerobic when necessary. Figure S1 in the Supporting Information shows the IR transmittance spectrum of the prism assembly with a water droplet on the reflection plane. At 2500−1800 and 900−350 cm^{-1}, transmittance decreased to less than 30% because of the absorption in diamond and water. Hence, absorbance spectra of the photocatalyst particles are shown herein in the wavenumber ranges of 6000−2500 and 1800−900 cm^{-1}. Figure S2 shows the absorbance spectra of water and other liquids examined using the ATR assembly. The acquisition time was 19 s per spectrum with a wavenumber resolution of 8 cm^{-1}.

The depth of IR light (wavelength: 1 μm) penetration into water, d, was estimated at 0.15 μm according to the formula

$$d = \frac{\lambda}{2\pi(n_{\text{diamond}}^2 \sin^2\theta - n_{\text{water}}^2)^{1/2}} \quad (1)$$

with θ = 45°, refractive index of diamond n_{diamond} = 2.38, and refractive index of water n_{water} = 1.32. The refractive index of water−photocatalyst mixtures should be greater than n_{water} to increase d accordingly, although the index of $NaTaO_3$ is unknown. $LiTaO_3$ exhibits an index of 2.14.[18]

$NaTaO_3$ and $KTaO_3$ photocatalysts were prepared and doped with Sr cations by a solid-state method according to studies reported earlier.[4,6] The atom number ratio of Na/Ta or K/Ta was set at 1.05 in the starting material to compensate for the possible sublimation of the alkali-metal elements during calcination. Excess alkali metals and doping metals (Sr or La) were removed by washing calcined particles with a dilute HCl solution (1 mol L^{-1}). The Sr concentrations of washed $NaTaO_3$ and washed $KTaO_3$ were determined to be 3.7 and 1.8 mol %, respectively, relative to the Ta cation concentrations using an X-ray fluorescence spectrometer (EDX-720, Shimadzu). Another $NaTaO_3$ photocatalyst was doped with La cations (La concentration: 2.7 mol %) in a similar manner. Their perovskite structures were examined and confirmed (Figure S3). The washed particles provided cubes with side lengths less than 1 μm (Figure S4). The $NaTaO_3$ ($KTaO_3$) photocatalysts doped with Sr or La cations exhibited a band gap of 4.1 (3.6) eV.[17] The Supporting Information lists the reagents used in preparing the photocatalysts and liquid droplets.

3. RESULTS AND DISCUSSION

3.1. Steady UV Irradiation under Water. $NaTaO_3$ particles doped with Sr cations (3.7 mol %) were placed on a reflection plane, which was covered with air-exposed water and irradiated with UV light. Spectrum a in Figure 1 shows the absorbance change (Δabsorbance) induced by steady irradiation (UV-light power: 19 W m^{-2}). An asymmetric absorption band with a maximum at 1400 cm^{-1} appeared in the nearly full wavenumber window of 5000−900 cm^{-1}. This absorption corresponds to the optical transition of photoexcited electrons, as described in Section 3.2. Negative peaks superimposed at 3700−3000 and 1600 cm^{-1} correspond to the vibrational absorption of water breached by UV irradiation. The breach peaks shifted to 2700−2500 and 1300 cm^{-1} as expected, in spectrum b recorded in D_2O.

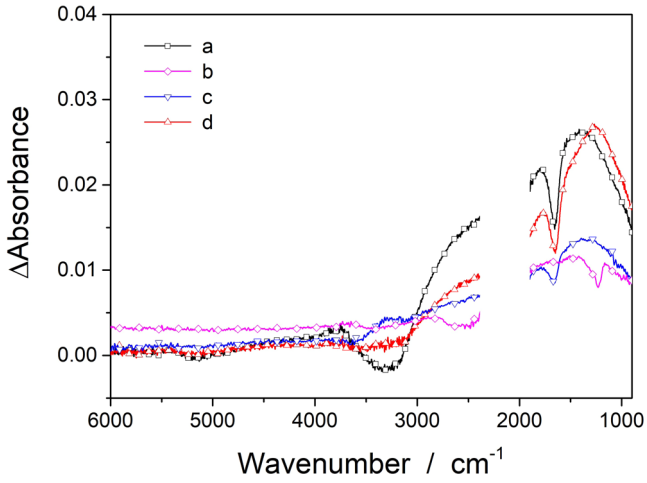

Figure 1. Absorbance change (Δabsorbance) of photocatalyst particles excited under water. Strontium-doped $NaTaO_3$ (Sr concentration: 3.7 mol %) exhibited spectrum a in H_2O and spectrum b in D_2O. Lanthanum-doped $NaTaO_3$ (La concentration: 2.7 mol %) exhibited spectrum c in H_2O. Spectrum d was observed for Sr-doped $KTaO_3$ (Sr concentration: 1.8 mol %) in H_2O. UV-light power: 19 W m^{-2}. The water droplets were exposed to air.

La-doped $NaTaO_3$ and Sr-doped $KTaO_3$ photocatalysts exhibited Δabsorbance spectra c and d, respectively. The asymmetric spectrum was a feature typical of metal-doped alkali-metal tantalates photoexcited under water. It was difficult to regulate the amount of photocatalyst particles placed in the volume probed with evanescent IR light. Hence, the absolute value of Δabsorbance is not compared for different photocatalysts.

3.2. Effect of an Electron or a Hole Scavenger. UV-light-induced absorbance change was further examined in the presence of reagents capable of scavenging excited electrons (e.g., $FeCl_3$, $NaIO_3$, and H_2O_2) or holes (e.g., methanol and Na_2SO_3) as summarized in Figure 2. In a droplet of methanol−water mixture (50 vol %) exposed to air, the asymmetric band (spectrum a in Figure 2) was enhanced by a factor of 2.7 compared with that observed in pristine water (spectrum c). The significant enhancement was ascribed to the hole-scavenging reaction by methanol, in spite of the unregulated amount of particles in the probed volume.

The enhanced absorption indicated that band-gap-excited electrons induce the asymmetric band. Under steady UV irradiation, the number of excited electrons and holes are regulated in their recombination. When holes are transferred to methanol,[19] the number of electrons should increase in the particles. Another hole scavenger, SO_3^{2-} (0.1 mol L^{-1}),

https://doi.org/10.1021/acs.jpcc.1c06618
J. Phys. Chem. C 2021, 125, 26398−26405

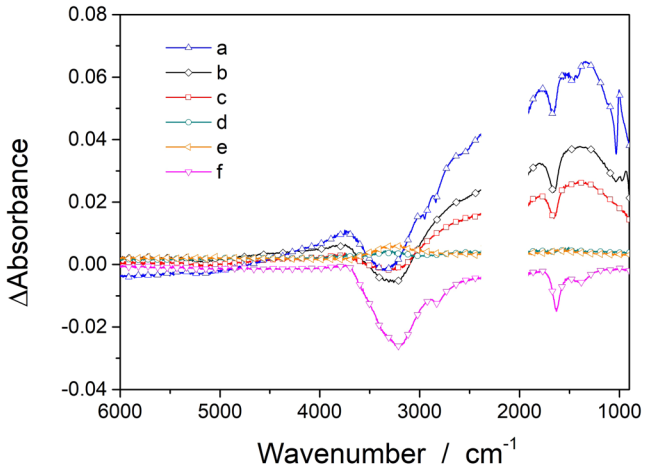

Figure 2. Absorbance change of Sr-doped $NaTaO_3$ (Sr concentration: 3.7 mol %) induced by UV-light irradiation. The particles were covered with air-exposed aqueous solutions of a: methanol, b: Na_2SO_3, c: water, d: $FeCl_3$, e: $NaIO_3$, and f: H_2O_2. UV-light power: 19 W m^{-2}. Spectrum a in Figure 1 was reproduced by spectrum c in this figure.

enhanced the absorbance change by a factor of 1.5 (spectrum b) to support the assignment to excited electrons.

On the other hand, the absorption disappeared in the case of solutions of $FeCl_3$ (0.05 mol L^{-1}) and $NaIO_3$ (0.05 mol L^{-1}), as shown by spectra d and e, respectively. Excited electrons were transferred to Fe^{3+}[20] or IO_3^-[21] in the solution. In addition, the absorption for a 15 vol % aqueous H_2O_2 solution disappeared (spectrum f). Hydrogen peroxide receives two electrons to produce water. The negative bands observed at 1300, 1600, 2800, and 3200 cm^{-1} corresponded to the vibrational absorption of H_2O_2 breached during the electron scavenging reaction.

According to the above-described results and interpretation, the UV-light-induced band at 5000−900 cm^{-1} corresponded to the excited electrons that have not yet recombined with holes. The electrons and holes were transferred to oxidative and reductive reagents across the particle−solution interface to modify their population in the particles.

3.3. Electron Decay Kinetics in Anaerobic Decane. The photoexcited electrons lived sufficiently long in the particles to produce their signature in the steady-state spectra. Thereafter, the decay kinetics of the electrons in the Sr-doped $NaTaO_3$ particles was examined by UV-light power dependence and time-resolved traces of deexcitation.

The Sr-doped $NaTaO_3$ particles were placed on the prism and covered with a droplet of *n*-decane. The spectrometer was then purged with N_2 to provide the least reactive liquid environment to the excited charge carriers, i.e., anaerobic decane. Figure 3a shows the Δabsorbance spectra recorded under UV light in the power range of 0.81−19 W m^{-2}, which corresponded to 1.2−27 photons s^{-1} nm^{-2}. The asymmetric spectrum at 5000−900 cm^{-1} was identical to that observed in water; hence, this spectrum is attributed to excited electrons. The absorption disappeared when I_2 (0.9 mmol L^{-1}) was dissolved in decane (Figure 3b). The removed absorption supports assignment to excited electrons due to iodine being a hole scavenger. The negative peaks at 3000−2800 and 1500−1300 cm^{-1} were breached vibrational bands of decane.

The inset plot shows a log−log plot of Δabsorbance at 1400 cm^{-1} as a function of light power, *P*. A straight line

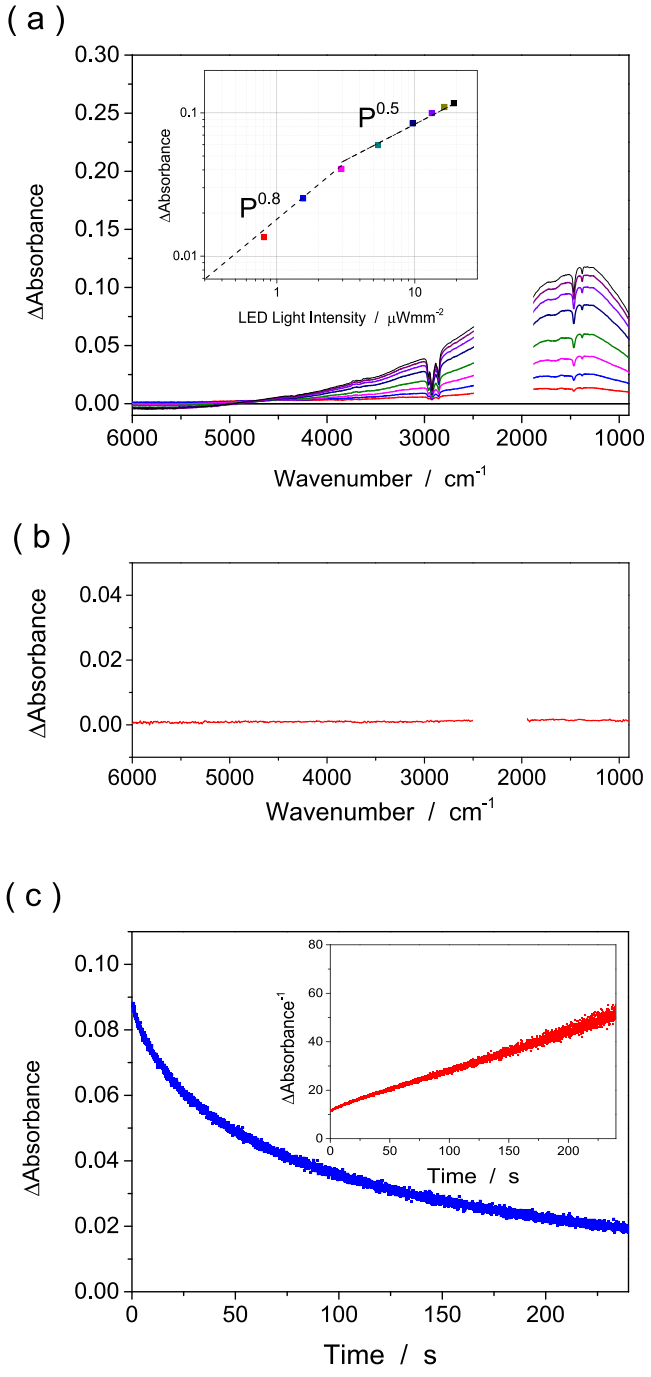

Figure 3. UV-light-induced IR absorption of Sr-doped $NaTaO_3$ (Sr concentration: 3.7 mol %) immersed in N_2-exposed decane. (a) Δabsorbance Spectra observed with UV-light powers of 0.81, 1.6, 2.9, 5.4, 9.6, 13, 16, and 19 W m^{-2}. The inset plots Δabsorbance at 1400 cm^{-1} as a function of light power. Broken lines show $P^{0.5}$ and $P^{0.8}$ laws fitted to the observations. (b) Δabsorbance Spectrum observed under UV irradiation (19 W m^{-2}) in I_2-containing decane. (c) Decay of Δabsorbance at 1400 cm^{-1} with excitation light (19 W m^{-2}) stopped at time zero. The inset shows the fitting to the second-order rate law to yield a gradient *k* of 0.16 ± 0.0[1] s^{-1}.

representing $P^{0.5}$ fitted the results observed with *P* greater than 5 W m^{-2}. The 1/2-order power law suggested deexcitation through recombination of electrons and holes. The number of excitation per second was proportional to *P*, while the deexcitation rate was expressed in terms of the

https://doi.org/10.1021/acs.jpcc.1c06618
J. Phys. Chem. C 2021, 125, 26398−26405

collision frequency of electrons and holes randomly migrating in the particle. The rates of excitation and deexcitation were balanced in the steady state

$$P \propto \text{electron excitation rate} = \text{electron deexcitation rate} = k_d[\text{electron}][\text{hole}] \quad (2)$$

with electron population [electron], hole population [hole], and deexcitation rate constant k_d. In the absence of a redox reaction on the particle surface, which should be the case in anaerobic decane, an equivalent number of electrons and holes were present in the particle, leading to the 1/2-order power law

$$P \propto k_d[\text{electron}]^2 \propto \Delta\text{absorbance}^2 \quad (3)$$

With the decrease in P to 1 W m^{-2}, the power law order gradually increased to 0.8. The increased order can be explained by the partial contribution of weak excitation, in which a limited number of electron−hole pairs, not excitons in the time scale examined in this study, were created in a particle. When neighboring electron−hole pairs were separated in space, the electron−hole collision frequency was proportional to the number of pairs [electron−hole pair], leading to the first-order power law

$$P \propto k'_d[\text{electron} - \text{hole pair}] \propto \Delta\text{absorbance} \quad (4)$$

The deexcitation rate was then traced with a time resolution of 50 ms by the rapid scanning of the interferometer. When UV-light irradiation was stopped at time zero, Δabsorbance at 1400 cm^{-1} gradually decreased over 200 s (Figure 3c). The inset plot revealed that reciprocal Δabsorbance linearly increases as a function of time with a gradient k of 0.16 ± 0.01 s^{-1}

$$\frac{1}{[\Delta\text{absorbance}(t)]} = \frac{1}{[\Delta\text{absorbance}(t=0)]} + kt \quad (5)$$

The linear relationship exhibited a second-order decay rate law according to the formula below, which is consistent with deexcitation via recombination observed in the UV-light power dependence.

$$\frac{d[\text{electron}]}{dt} = -k_d[\text{electron}]^2 \quad (6)$$

The rate constant k_d is expressed as mol^{-1} s^{-1}, when the number of electrons in the probed volume is quantified in mol. In this study, the number of excited electrons was quantified by IR light absorbance. As absorbance is dimensionless, the rate constant k in eq 5 is expressed in s^{-1}. The molar absorption coefficient for excited electrons is not known and k_d cannot be determined.

One may suppose that deexcitation rate should deviate from the second-order rate law with charge-carrier density decreased enough since steady Δabsorbance was proportional to $P^{0.8}$ with small light powers. The authors assume that the second-order deexcitation occurs even when the carrier density decreases to a number with which the first-order, pair recombination would take place under steady light irradiation. This is because the spatial distribution of electrons and holes should be randomized during the second-order deexcitation. The first-order, pair recombination requires collision of an electron and a hole that were created by one same photon. This requirement is not filled in deexcitation initiated with a large number of electrons and holes.

The authors attempted to fit the Δabsorbance decay to straight lines in a semi-log or log−log plot but failed (Figure S5). Hence, a single exponential or polynomial function does not represent decay kinetics. Fitting to stretched exponential functions proportional to e^{-kt^β} with $\beta < 1$ was not examined since this class of functions cannot predict the steady-state electron population. When excited electrons decay as

$$[\text{electron}(t)] = [\text{electron}(t=0)]\cdot e^{-kt^\beta} \quad (7)$$

its time derivative is expressed as follows

$$-k\beta\cdot[\text{electron}(t)]\cdot t^{\beta-1} \quad (8)$$

In the steady state, the time derivative should be balanced with the number of excitation per second. However, the formulated derivative explicitly involves variable t in addition to [electron(t)]. This failure indicates that stretched exponential functions are beneficial for describing transient kinetics, not steady-state kinetics. The electron population traced in Figure 3c was in the steady state until excitation light was turned off. Hence, the deexcitation kinetics should be formulated to be consistent with the steady-state population. This requirement was not satisfied with stretched exponential functions although the functions were established in the recombination rate controlled by the defect trapping of excited charge carriers.

3.4. Electron Decay Kinetics in Anaerobic Water. Finally, excited-electron decay was examined in water, where overall water splitting would contribute to electron decay. The spectrometer was purged with N_2 to minimize the concentration of O_2, an electron scavenger in the water droplet.

Figure 4a shows the light-power dependence of Δabsorbance at 1400 cm^{-1}. Again, it was proportional to $P^{0.5}$ in the entire power range of 0.8−19 W m^{-2} (shown in the inset), whereas the absorption strength was less than that observed in decane. The reduced strength suggested that electrons are consumed in water-related reactions. However, the amount of particles in the probed volume might have been different in the two series of measurements (Figures 3 and 4). Light penetration depth was controlled by the refractive index of the liquid−particle mixture, which was not necessarily identical in decane and water.

Hence, the electron decay rate is evaluated by the time-resolved trace of Δabsorbance. Panel (b) shows the Δabsorbance at 1400 cm^{-1} as a function of time observed in anaerobic water. Reciprocal Δabsorbance observed at 50−200 s was fitted to a linear line to indicate a second-order decay rate law, which was consistent with the 1/2-order power law of the light-power dependence. The gradient in the linear reciprocal plot was 0.35 ± 0.10 s^{-1} greater than that in decane by a factor of 2. Single exponential and polynomial functions failed to fit the observed Δabsorbance (Figure S6). Another Δabsorbance trace observed on a different day is available in Figure S7 to certify experimental reproducibility. The reason of the greater gradient in water, which suggested accelerated recombination, is not known.

The observations at 0−50 s deviated from the linear relation, making the trace convex upward. The convex trace indicates that the electron number decreases more rapidly than that predicted by the second-order decay rate law. One possible reason for decay acceleration at 0−50 s is the consumption of electrons in the water-splitting reaction on the particles.

The apparent quantum yield of the water-splitting reaction, which is defined as the ratio of the number of electrons

https://doi.org/10.1021/acs.jpcc.1c06618
J. Phys. Chem. C 2021, 125, 26398−26405

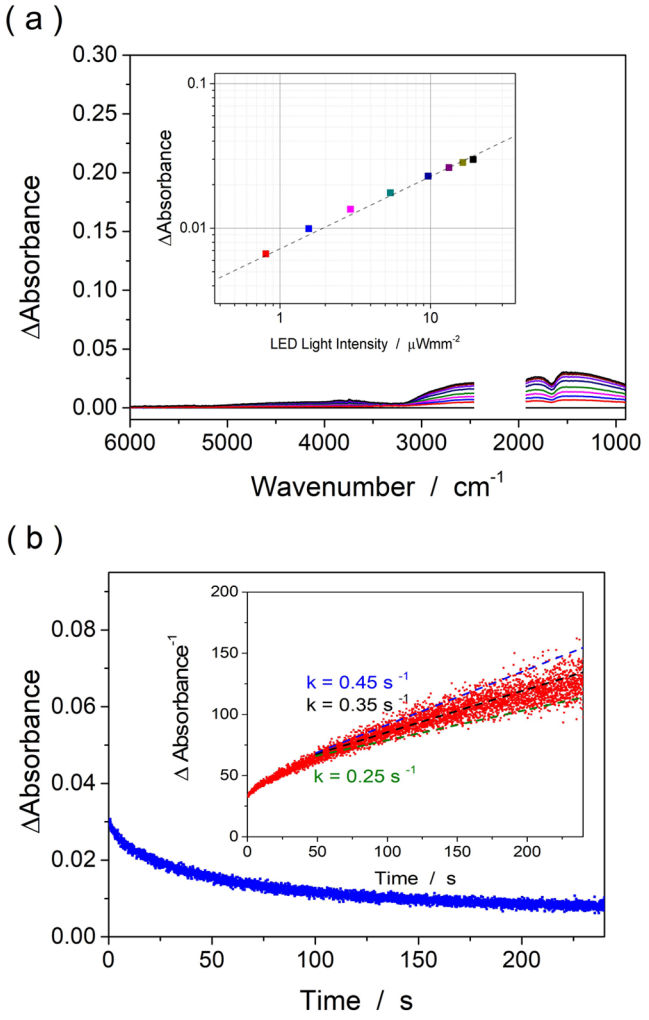

Figure 4. UV-light-induced IR absorption of Sr-doped $NaTaO_3$ (Sr concentration: 3.7 mol %) immersed in N_2-exposed water. (a) Δabsorbance spectra observed with UV-light powers of 0.81, 1.6, 2.9, 5.4, 9.6, 13, 16, and 19 W m^{-2}. The inset plots Δabsorbance at 1400 cm^{-1} as a function of light power. The broken line shows a 1/2-order power law fitted to the observations. (b) Decay of Δabsorbance at 1400 cm^{-1} when excitation light (19 W m^{-2}) was turned off at time zero. The inset shows fitting to a second-order rate law to yield a gradient of 0.35 ± 0.10 s^{-1}.

consumed in the desired photocatalytic reaction to the number of incident photons, was not quantified for the photocatalysts examined herein. Iwase et al.[22] have reported that a similarly prepared Sr-doped $NaTaO_3$ photocatalyst (Sr concentration: 5 mol %) produces 0.6 mmol h^{-1} of H_2. The same research group has reported a H_2 production rate of 19.8 mmol h^{-1} on a La-doped photocatalyst modified with a NiO cocatalyst, which afforded a yield of 56%.[23] Hence, the authors estimate yield in the order of 1% on our Sr-doped $NaTaO_3$ photocatalyst. The estimated yield suggests active water splitting on the particles. Often, hydrogen and oxygen bubbles were visible on the water-splitting photocatalysts with a yield greater than 10%. Actually, UV-light-induced Δabsorbance of metal-doped $NaTaO_3$ photocatalysts exhibited a linear relation with the rate of photocatalytic H_2 production in an earlier study.[24] Hence, the authors suggest a principal role of the electrons detected by IR absorption in the water splitting reaction.

When the authors ascribe Δabsorbance decay accelerated at 0−50 s to electron consumption in the water splitting reaction, they should further infer that the probability for an electron to react with water decreased as electron density decreased below a threshold density quantified with Δabsorbance at 50 s. Though the reason of decreased probability is not known in the Sr-doped $NaTaO_3$ photocatalyst, reaction probability sensitive to charge-carrier density has been found on a number of metal oxide semiconductors. A first-order reaction at low hole densities switched to a faster, third-order reaction at higher hole densities in photoelectrochemical oxidation of water on TiO_2, $BiVO_4$, Fe_2O_3, and WO_3.[25] Transition from the first-order reaction to third-order reaction was related to the quasi-Fermi level of excited holes. In photocatalytic water oxidation on $SrTiO_3$ doped with Al cations,[26] the photocatalyst was inactive for O_2 evolution when excitation light was turned on. Charge carriers produced by first absorbed photons were consumed for activating the photocatalyst and then latter photons drove steady O_2 evolution on the activated photocatalyst. The electron-induced, H_2 evolution reaction on Sr-doped $NaTaO_3$ may provide another case of reaction probability sensitive to charge-carrier density.

3.5. Comparison with Δabsorbance in Vacuum. In an earlier paper,[4] the authors investigated the IR absorption of Sr-doped $NaTaO_3$ particles excited in vacuum, where UV-light-induced absorbance change was recorded with the IR light transmitted through the particles. The Δabsorbance spectra observed in vacuum exhibited a gradual rise at 5000 cm^{-1} to a plateau at 3000−1400 cm^{-1} and terminated with a sharp peak at 1000 cm^{-1}. A Δabsorbance spectrum observed on Sr-doped $NaTaO_3$ (Sr concentration: 4.7 mol %) placed in vacuum is quoted from ref 4 and reproduced in Figure 5 (spectrum a) to compare with those observed under water and decane in the present study (spectra b and c, respectively).

In ref 4, the authors assigned the Δabsorbance spectrum as a whole to electrons excited and not yet recombined based on the response to O_2 (an electron scavenger) or methanol vapor (a hole scavenger). The three spectra compared in Figure 5 led us to revisit the assignment; the spectrum in vacuum revealed two absorption bands as depicted in the inset figure. Broad absorption with a maximum at 1400 cm^{-1} was observed in vacuum (spectrum a) and also in liquid (spectra b and c). The full width at half-maximum (FWHM) was estimated at 2500 cm^{-1}, though the low-wavenumber end of the spectra was out of the wavenumber window. Another feature, peaked absorption at 1000 cm^{-1}, solely appeared in vacuum but absent in liquid. Its FWHM was about 300 cm^{-1}. The revisited assignment indicates two types of excited electrons in the photocatalyst particles, one sensitive and the other insensitive to the presence of liquid over the particles.

Here, the authors hypothesize the origin of the Δabsorbance induced by UV-light irradiation. When an electron is excited across the band gap and then accommodated in a spatially confined, mid-gap state, its photoexcitation to the conduction band affords an asymmetric absorption band. The low-energy threshold for the optical transition is determined by the energy gap between the mid-gap state and conduction-band minimum according to the Franck−Condon principle.

Absorption coefficient decreases with photon energy over the threshold to make a peak at wavenumbers close to the threshold. This is because the initial state is confined in real space and thus limited in momentum space. The probability of optical transition decreases with electron momentum required

https://doi.org/10.1021/acs.jpcc.1c06618
J. Phys. Chem. C 2021, 125, 26398−26405

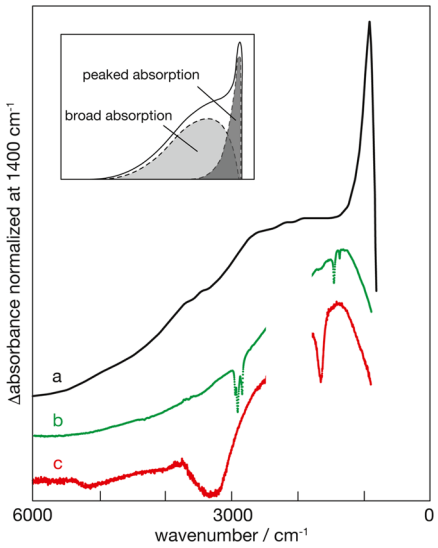

Figure 5. UV-light-induced IR absorption on Sr-doped $NaTaO_3$ particles observed in different environments. a: Sr-doped $NaTaO_3$ (Sr concentration: 4.7 mol %) were placed in vacuum and irradiated with a Hg−Xe lamp. b and c: Sr-doped $NaTaO_3$ (Sr concentration: 3.8 mol %) were irradiated in air-exposed water and N_2-exposed decane, respectively. The three spectra were normalized at 1400 cm^{-1} and depicted by vertical offsets for comparison. Spectrum h in Figure 7 in ref 4 is reproduced as spectrum a in this figure. Spectra b and c in this figure reproduce spectrum a in Figure 1 and the most intense spectrum in Figure 3 in this paper, respectively. The inset depicts two absorptions revealed in spectrum a.

in the final state, i.e., electron energy in the final state. Shallow donor/acceptor states in covalent semiconductors provide well-known examples of state-to-band transition. Boron-doped Si exhibited asymmetric absorption peaked at 400 cm^{-1} with an FWHM of 400 cm^{-1}, according to Figures 3−30 in ref 27.

The Δabsorbance of Sr-doped $NaTaO_3$ peaked at 1000 cm^{-1}, which was observed solely in vacuum, is fully consistent to the features described in the preceding paragraph including the peak wavenumber and peak width. The absorption is therefore assigned to electron transition from a spatially confined, mid-gap state to the conduction band. Furthermore, the initial state should have been localized on the surface of photocatalyst particles to make the absorption sensitive to the environment. As a surface electronic state is partially distributed in vacuum, its spatial distribution and eigenenergy can be modified or even quenched by the surrounding liquid.

On the other hand, the broad absorption with a maximum at 1400 cm^{-1} appeared in vacuum and liquid. Electron transition causing the absorption occurred in the particles away from the environment. Δabsorbance decreased with wavenumber above 1400 cm^{-1} as expected in state-to-band transition. However, the FWHM of this absorption, 2500 cm^{-1}, was definitely larger than that of the peaked absorption. The large bandwidth suggests a different character, possibly different extent of confinement, of the mid-gap state for the broad absorption from that for the peaked absorption.

Currently, the nature of the two mid-gap states hypothesized herein is not known; electron trapping in intrinsic unoccupied states in the band gap and self-trapping in an otherwise perfect lattice are equally possible. In the latter form of trapping, the ionic semiconductor lattice is deformed around an excited electron to create a polaron; the excess electron is self-trapped in a Coulombic potential well, which is produced by the shifting of ions from their equilibrium positions.[28] Theoretical studies have emphasized the role of polarons in the control of the carrier transport rate in the bulk[29−32] and modification of the overpotentials of surface redox reactions.[33−36] A limited number of experimental studies have focused on polarons in binary metal oxides for photocatalyst models, e.g., TiO_2,[37−39] ZnO,[40] and Fe_2O_3.[41,42] Future study is required to reveal the identity and role of the mid-gap states in alkali-metal tantalate photocatalysts modified with metal doping.

4. CONCLUSIONS

Long-life electrons band-gap-excited in alkali-metal tantalate photocatalysts feasible for overall water splitting were investigated. $NaTaO_3$ and $KTaO_3$ photocatalysts doped with Sr or La cations exhibited IR absorption when the band gap was excited under water and decane. The broad, asymmetric absorption with a maximum at 1400 cm^{-1} corresponded to excited electrons according to the response to the scavenging reagents. The excited electrons were accommodated in mid-gap states, and the photoexcitation of the accommodated electrons afforded a broad absorption band. The mid-gap states were supposed to be present in the bulk particles as the IR absorption spectrum was insensitive to the environment, vacuum or liquid, surrounding the particles. The electron population decayed through recombination of electrons and holes along a second-order rate law. The population decay was accelerated in water; this is possibly related to a water-related electron-consuming reaction. The ATR-based method demonstrated in this study is applicable to several other photofunctional materials in liquid.

■ ASSOCIATED CONTENT

Supporting Information

The Supporting Information is available free of charge at https://pubs.acs.org/doi/10.1021/acs.jpcc.1c06618.

Reagents, IR absorption spectra of the prism assembly (Figure S1) and liquid droplets (Figure S2), X-ray diffraction patterns (Figure S3) and scanning electron micrographs (Figure S4) of the photocatalyst particles, semi-log and log−log plots of electron decay in anaerobic decane (Figure S5) and anaerobic water (Figure S6), and another Δabsorbance trace in anaerobic water (Figure S7) (PDF)

■ AUTHOR INFORMATION

Corresponding Authors

Zhebin Fu − *Department of Chemistry, School of Science, Kobe University, Kobe 657-8501, Japan;* orcid.org/0000-0003-1017-4955; Email: fu@harbor.kobe-u.ac.jp

Hiroshi Onishi − *Department of Chemistry, School of Science, Kobe University, Kobe 657-8501, Japan;* orcid.org/0000-0003-1873-9105; Email: oni@kobe-u.ac.jp

Author

Takuya Hirai − *Department of Chemistry, School of Science, Kobe University, Kobe 657-8501, Japan*

Complete contact information is available at: https://pubs.acs.org/10.1021/acs.jpcc.1c06618

Author Contributions

The manuscript was written through contributions of all authors.

Notes

The authors declare no competing financial interest.

■ ACKNOWLEDGMENTS

The authors thank Ryosuke Matsubara for his advice with respect to the selection of electron scavenging reagents. This study was supported by JSPS KAKENHI (grant numbers JP19H00915 and 18KK0161).

■ REFERENCES

(1) Wang, Q.; Domen, K. Particulate Photocatalysts for Light-Driven Water Splitting: Mechanisms, Challenges, and Design Strategies. *Chem. Rev.* **2020**, *120*, 919−985.
(2) Kranz, C.; Wächtler, M. Characterizing photocatalysts for water splitting: from atoms to bulk and from slow to ultrafast processes. *Chem. Soc. Rev.* **2021**, *50*, 1407−1437.
(3) Takanabe, K. Addressing fundamental experimental aspects of photocatalysis studies. *J. Catal.* **2019**, *370*, 480−484.
(4) An, L.; Onishi, H. Electron-Hole Recombination Controlled by Doping Sites in Perovskite-Structured Photocatalysts: Sr-Doped $NaTaO_3$. *ACS Catal.* **2015**, *5*, 3196−3206.
(5) Yamakata, A.; Ishibashi, T.; Kato, H.; Kudo, A.; Onishi, H. Photodynamics of $NaTaO_3$ Catalysts for Efficient Water Splitting. *J. Phys. Chem. B* **2003**, *107*, 14383−14387.
(6) Sudrajat, H.; Dhakal, D.; Kitta, M.; Sasaki, T.; Ozawa, A.; Babel, S.; Yoshida, T.; Ichikuni, N.; Onishi, H. Electron Population and Water Splitting Activity Controlled by Strontium Cations Doped in $KTaO_3$ Photocatalysts. *J. Phys. Chem. C* **2019**, *123*, 18387−18397.
(7) Yoshihara, T.; Katoh, R.; Furube, A.; Tamaki, Y.; Murai, M.; Hara, K.; Murata, S.; Arakawa, H.; Tachiya, M. Identification of Reactive Species in Photoexcited Nanocrystalline TiO_2 Films by Wide-Wavelength-Range (400−2500 nm) Transient Absorption Spectroscopy. *J. Phys. Chem. B* **2004**, *108*, 3817−3823.
(8) Tang, J.; Durrant, J. R.; Klug, D. R. Mechanism of Photocatalytic Water Splitting in TiO_2. Reaction of Water with Photoholes, Importance of Charge Carrier Dynamics, and Evidence for Four-Hole Chemistry. *J. Am. Chem. Soc.* **2008**, *130*, 13885−13891.
(9) Le Formal, F.; Pastor, E.; Tilley, S. D.; Mesa, C. A.; Pendlebury, S. R.; Grätzel, M.; Durrant, J. R. Rate Law Analysis of Water Oxidation on a Hematite Surface. *J. Am. Chem. Soc.* **2015**, *137*, 6629−6637.
(10) Ma, Y.; Pendlebury, S. R.; Reynal, A.; Le Formal, F.; Durrant, J. R. Dynamics of photogenerated holes in undoped $BiVO_4$ photoanodes for solar water oxidation. *Chem. Sci.* **2014**, *5*, 2964−2973.
(11) Nakamura, R.; Nakato, Y. Primary Intermediates of Oxygen Photoevolution Reaction on TiO_2 (Rutile) Particles, Revealed by in Situ FTIR Absorption and Photoluminescence Measurements. *J. Am. Chem. Soc.* **2004**, *126*, 1290−1298.
(12) Sivasankar, N.; Weare, W. W.; Frei, H. Direct Observation of a Hydroperoxide Surface Intermediate upon Visible Light-Driven Water Oxidation at an Ir Oxide Nanocluster Catalyst by Rapid-Scan FT-IR Spectroscopy. *J. Am. Chem. Soc.* **2011**, *133*, 12976−12979.
(13) Zhang, M.; de Respinis, M.; Frei, H. Time-resolved observations of water oxidation intermediates on a cobalt oxide nanoparticle catalyst. *Nat. Chem.* **2014**, *6*, 362−367.
(14) Herlihy, D. M.; Waegele, M. M.; Chen, X.; Pemmaraju, C. D.; Prendergast, D.; Cuk, T. Detecting the oxyl radical of photocatalytic water oxidation at an n-$SrTiO_3$/aqueous interface through its subsurface vibration. *Nat. Chem.* **2016**, *8*, 549−555.
(15) Zandi, O.; Hamann, T. W. Determination of photoelectrochemical water oxidation intermediates on haematite electrode surfaces using operando infrared spectroscopy. *Nat. Chem.* **2016**, *8*, 778−783.
(16) Chen, T.; Ding, Q.; Wang, X.; Feng, Z.; Li, C. Mechanistic Studies on Photocatalytic Overall Water Splitting over Ga_2O_3-Based Photocatalysts by *Operando* MS-FTIR Spectroscopy. *J. Phys. Chem. Lett.* **2021**, *12*, 6029−6033.
(17) Onishi, H. Sodium Tantalate Photocatalysts Doped with Metal Cations: Why Are They Active for Water Splitting? *ChemSusChem* **2019**, *12*, 1825−1834.
(18) Refractive Index at 1 μm Wavelength of Diamond, Water, and $LiTaO_3$ was Quoted From. In *CRC Handbook of Chemistry and Physics*, 92nd ed.; Haynes, W. M.; Lide, D. R., Eds.; CRC Press: Boca Raton, FL, 2011.
(19) Yamakata, A.; Ishibashi, T.; Onishi, H. Electron- and Hole-Capture Reactions on Pt/TiO_2 Photocatalyst Exposed to Methanol Vapor Studied by Time-Resolved Infrared Absorption Spectroscopy. *J. Phys. Chem. B* **2002**, *106*, 9122−9125.
(20) Ohno, T.; Haga, D.; Fujihara, K.; Kaizaki, K.; Matsumura, M. Unique Effects of Iron(III) Ions on Photocatalytic and Photoelectrochemical Properties of Titanum Dioxide. *J. Phys. Chem. B* **1997**, *101*, 6415−6419.
(21) Sayama, K.; Mukasa, K.; Abe, R.; Abe, Y.; Arakawa, H. Stoichiometric water splitting into H_2 and O_2 using a mixture of two different photocatalysts and an IO_3^-/I^- shuttle redox mediator under visible light irradiation. *Chem. Commun.* **2001**, 2416−2417.
(22) Iwase, A.; Kato, H.; Kudo, A. The Effect of Alkaline Earth Metal Ion Dopants on Photocatalytic Water Splitting by $NaTaO_3$ Powder. *ChemSusChem* **2009**, *2*, 873−877.
(23) Kato, H.; Asakura, K.; Kudo, A. Highly Efficient Water Splitting into H_2 and O_2 over Lanthanum-Doped $NaTaO_3$ Photocatalysts with High Crystallinity and Surface Nanostructure. *J. Am. Chem. Soc.* **2003**, *125*, 3082−3089.
(24) Maruyama, M.; Iwase, A.; Kato, H.; Kudo, A.; Onishi, H. Time-Resolved Infrared Absorption Study of $NaTaO_3$ Photocatalysts Doped with Alkali Earth Metals. *J. Phys. Chem. C* **2009**, *113*, 13918−13923.
(25) Mesa, C. A.; Francàs, L.; Yang, K. R.; Garrido-Barros, P.; Pastor, E.; Ma, Y.; Kafizas, A.; Rosser, T. E.; Mayer, M. T.; Reisner, E.; et al. Multihole Water Oxidation Catalysis on Haematite Photoanodes Revealed by Operando Spectroelectrochemistry and DFT. *Nat. Chem.* **2020**, *12*, 82−89.
(26) Kosaka, T.; Teduka, Y.; Ogura, T.; Zhou, Y.; Hisatomi, T.; Nishiyama, H.; Domen, K.; Takahashi, Y.; Onishi, H. Transient Kinetics of O_2 Evolution in Photocatalytic Water-Splitting Reaction. *ACS Catal.* **2020**, *10*, 13159−13164.
(27) Pankove, J. I. *Optical Processes in Semiconductors*; Dover: New York, 1975.
(28) Emin, D. Optical properties of large and small polarons and bipolarons. *Phys. Rev. B* **1993**, *48*, 13691−13702.
(29) Deskins, N. A. Electron transport via polaron hopping in bulk TiO_2: a density functional theory characterization. *Phys. Rev. B* **2007**, *75*, No. 195212.
(30) Di Valentin, C.; Selloni, A. Bulk and Surface Polarons in Photoexcited Anatase TiO_2. *J. Phys. Chem. Lett.* **2011**, *2*, 2223−2228.
(31) Davies, D. W.; Savory, C. N.; Frost, J. M.; Scanlon, D. O.; Morgan, B. J.; Walsh, A. Descriptors for electron and hole charge carriers in metal oxides. *J. Phys. Chem. Lett.* **2020**, *11*, 438−444.
(32) Uratani, H.; Nakai, H. Simulating the Coupled Structural−Electronic Dynamics of Photoexcited Lead Iodide Perovskites. *J. Phys. Chem. Lett.* **2020**, *11*, 4448−4455.
(33) Ji, Y.; Wang, B.; Luo, Y. Location of trapped hole on rutile-TiO_2(110) surface and its role in water oxidation. *J. Phys. Chem. C* **2012**, *116*, 7863−7866.
(34) Di Valentin, C. A mechanism for the hole-mediated water photooxidation on TiO_2(1 0 1) surfaces. *J. Phys.: Condens. Matter* **2016**, *28*, No. 074002.
(35) Gono, P.; Wiktor, J.; Ambrosio, F.; Pasquarello, A. Surface Polarons Reducing Overpotentials in the Oxygen Evolution Reaction. *ACS Catal.* **2018**, *8*, 5847−5851.
(36) Govind Rajan, A.; Martirez, J. M. P.; Carter, E. A. Why do we use the materials and operating conditions we use for heterogeneous (photo)electrochemical water splitting. *ACS Catal.* **2020**, *10*, 11177−11234.
(37) Panayotov, D. A.; Burrows, S. P.; Morris, J. R. Infrared spectroscopic studies of conduction band and trapped electrons in

https://doi.org/10.1021/acs.jpcc.1c06618
J. Phys. Chem. C 2021, 125, 26398−26405

UV-photoexcited, H-atom n-doped, and thermally reduced TiO_2. *J. Phys. Chem. C* **2012**, *116*, 4535−4544.
(38) Sezen, H.; Buchholz, M.; Nefedov, A.; Natzeck, C.; Heissler, S.; Di Valentin, C.; Wöll, C. Probing electrons in TiO_2 polaronic trap states by IR-absorption: evidence for the existence of hydrogenic states. *Sci. Rep.* **2015**, *4*, No. 3808.
(39) Savory, D. M.; McQuillan, A. J. IR spectroscopic behavior of polaronic trapped electrons in TiO_2 under aqueous photocatalytic conditions. *J. Phys. Chem. C* **2014**, *118*, 13680−13692.
(40) Sezen, H.; Shang, H.; Bebensee, F.; Yang, C.; Buchholz, M.; Nefedov, A.; Heissler, S.; Carbogno, C.; Scheffler, M.; Rinke, P.; et al. Evidence for photogenerated intermediate hole polarons in ZnO. *Nat. Commun.* **2015**, *6*, No. 6901.
(41) Bandaranayake, S.; Hruska, E.; Londo, S.; Biswas, S.; Baker, L. R. Small polarons and surface defects in metal oxide photocatalysts studied using XUV reflection−absorption spectroscopy. *J. Phys. Chem. C* **2020**, *124*, 22853−22870.
(42) Shelton, J. L.; Knowles, K. E. Thermally Activated Optical Absorption into Polaronic States in Hematite. *J. Phys. Chem. Lett.* **2021**, *12*, 3343−3351.

https://doi.org/10.1021/acs.jpcc.1c06618
J. Phys. Chem. C 2021, 125, 26398−26405